Non-Parametric Object-Based Approaches to Carry Out ISA Classification From Archival Aerial Orthoimages

Ismael Fernández Luque, Fernando J. Aguilar, M. Flor Álvarez, and Manuel Ángel Aguilar

***Abstract*—In order to map the impervious surfaces for a coastal area, three non-parametric approaches: Classification and Regression Trees, Nearest Neighbor (NN), and Support Vector Machines (SVM)- were applied to a dataset of very high resolution archival orthoimages which had poor radiometry, with only red, green and blue spectral information. An object-based image analysis was carried out and four feature vectors were defined as input data for the classifier: 1) red, green and blue spectral information plus four relative spectral indices; 2) Dataset 1 plus texture indices based on the grey level co-occurrence matrix (GLCM); 3) Dataset 1 plus texture indices based on the local variance; and 4) the vector defined by 1), 2) and 3). Two classification strategies were developed in order to identify the pervious/impervious target classes (aggregation of all the subclasses and binary classification). The separability matrix was used to present the statistical comparative results clearly and concisely. The results obtained from this work showed that 1) "GLCM" texture indices did not lead to more accurate results; 2) the incorporation of the local variance texture index significantly increased the accuracy of the classification; 3) the classification results were not significantly affected by the classification strategy employed; 4) SVM and NN achieved statistically more accurate classification results than CARTs; 5) the SVM classifier was more efficient than the NN classifier, while NN was less dependent on the feature vector, and 6) suitable accuracy results were obtained for the most accurate approaches (SVM) which achieved a 89.4% overall accuracy.**

***Index Terms*—Archival orthoimages, impervious surface area (ISA), nearest neighbor (NN), non-parametric classifiers, object based image analysis (OBIA), support vector machines (SVMs), texture features.**

I. Introduction

IMPERVIOUS areas are defined as anthropogenic features through which water cannot infiltrate into the soil [1], [2] such as rooftops, pavements, roads, sidewalks, thus being a good indicator of the degree of urbanization in an area. The impervious surface areas (ISA) influence the hydrology of a watershed and have an impact on the potential volume increase, duration, and intensity of runoff and also affect the quantity of groundwater and increase stormflow [3]. An often overlooked environmental problem which is caused by ISA is the increase in runoff volume and discharge rate, in conjunction with non-point source pollution, which alter in-stream and riparian habitats [4]. Additionally, it increases the risk of erosion and habitat degradation. Those are the reasons why the percentage of ISA in a watershed is considered to be a basic indicator for the evaluation of non-point runoff and an estimate of the future available water quality [4]. Moreover, ISA show different thermal properties compared to pervious ones [1], [5], since they retain more heat than natural surfaces and therefore the stream temperature could potentially increase up to 6.5 degrees Celsius [6]. According to [6] and [7] the percentage of impervious surface area in a watershed is frequently correlated with the health of the ecosystem which the stream flows through. In this sense the ecosystem can be classified as stressed (up to 10% of the total surface area is impervious), impacted (between 11 and 25%) and degraded (more than 25%).

Taking into account all the aforementioned reasons, efficient techniques to accurately determine and map ISA should be developed. In this context, a remote sensing approach offers an appropriate and efficient alternative to identify impervious/pervious surfaces instead of using other labor-intensive approaches such as manually digitizing digital orthoimages [5], [8] or land surveying using GPS receivers. During the first decade of the 21st century, there has been an increase in studies related to both very high spatial resolution imagery and classification methods based on texture. According to [1], the considerations to keep in mind when implementing an ISA classification using digital images are: 1) spatial resolution; 2) geometric characteristics of urban features; 3) spectral resolution; and 4) temporal resolution.

The very high spatial resolution of images from satellites such as IKONOS, QuickBird, GeoEye-1 or WorldView-2 have enabled the accurate classification of relatively small size elements and the suitable extraction of ISA [9]–[11]. Furthermore, the orthoimages acquired from airborne platforms are regularly produced by government programmes (e.g., National Plan of Aerial Orthoimage, Spain, or National Digital Orthophoto Program, USA) constitute an archival data source which enables multitemporal land-use change studies and/or ISA detection [12] without the need for new data acquisition. While the current orthoimages usually include additional information such as the

Manuscript received November 28, 2012; revised January 10, 2013; accepted January 11, 2013. Date of publication January 30, 2013; date of current version July 22, 2013. This work was supported by Andalusia Regional Government, Spain, through the Excellence Research Project RNM-3575. This is a research project co-financed by the European Union through the program European Regional Development Fund. The authors appreciate the additional support from the Spanish Ministry under Grant Reference CTM2010-16573.

I. Fernández Luque is with the Department of Engineering, Area of Graphic Engineering, University of Almeria, Spain (corresponding author, e-mail: ismaelf@ual.es).

F. J. Aguilar and M. Á. Aguilar are with the Department of Engineering, Area of Graphic Engineering, University of Almeria, Spain (e-mail: faguilar@ual.es; maguilar@ual.es).

M. F. Álvarez is with the Department of Mining Engineering, Area of Topographic, Geodesy and Photogrammetric Engineering, University of Leon, Spain (e-mail: flor.alvarez@unileon.es).

Color versions of one or more of the figures in this paper are available online at http://ieeexplore.ieee.org.

Digital Object Identifier 10.1109/JSTARS.2013.2240265

near infrared band [2] or ancillary data (e.g., LiDAR data [13]), most of the archival orthoimages offered by the administration provide only information for the three regions of the visible spectrum red, green and blue (RGB). Additionally, archival images can have some artefacts, sometimes due to them not being carefully preserved. Therefore, since little spectral information is available, the identification of ISA from archival orthoimages is challenging. In order to obtain accurate results, the use of additional or ancillary information from GIS databases or image data fusion [1] is needed. Moreover, contextual information [14] and image texture analysis [15] have been considered helpful. The development of an efficient and accurate ISA classification method from very high spatial resolution RGB imagery would add value to the available archival data as a source of information for land-use change detection, coastal areas evolution, or urban monitoring.

Since the spatial resolution of the orthoimagery derived from photogrammetric flights is usually very high (0.20 – 1 m), it is appropriate to use an OBIA (object-based image analysis) approach. In fact, a higher local variance of urban land cover classes is found when the resolution of the input image is increased [16], and therefore, the accuracy of the traditional pixel-based classification approaches is reduced and the results could show a "salt and pepper" effect [17], [18]. Classification accuracy is particularly problematic in urban environments, which typically consist of mosaics of small features made up of materials with different physical properties. To overcome this problem, OBIA has been recognized as an approach that can help improve the performance of supervised classifiers [16], [19]–[22]. In fact, OBIA is a new paradigm in the field of geographic information science in which images are segmented into meaningful segments (or objects) according to different criteria before classification is carried out. The OBIA methodology is based on aggregating similar pixels in order to obtain homogenous objects, which are then assigned to a target class. Using objects instead of pixels as a minimum unit of information minimizes the "salt-pepper" effect due to the spectral heterogeneity of individual pixels. Furthermore, and unlike traditional pixel-based methods which only use spectral information, object-based approach can use shape, texture and context information associated with the objects and thus it has the potential to efficiently handle more difficult image analysis tasks. Moreover, this object-oriented approach enables the use of hierarchical classifications at different scales [23]. In this way, the amount of available OBIA works is increasing rapidly and there are numerous empirical studies published in peer-reviewed journals which have provided sufficient evidence of the advantages of object-based classification over traditional pixel-based classification (e.g., [16], [20], [21], [24]–[28]). A comprehensive review of the advantages and the disadvantages of using OBIA approach for image classification as well as the state of the art of these methods can be found in [22].

Taking into account all the aforementioned explanations regarding the application of OBIA methodology on high resolution images, the main goal of this work was to identify and map impervious and pervious surfaces of a coastal area using an OBIA approach and RGB archival orthoimages from a photogrammetric flight without any other ancillary information. Three non-parametric classification methods—Classification and Regression Trees (CART), Nearest Neighbor (NN) and Support Vector Machines (SVM)—were tested in order to avoid assumptions about the distribution of the data. The three methods, which will be described in the following section, are widely known and used for image classification in remote sensing [29]–[32]. Furthermore, four different features sets were used in the classification in order to determine the most suitable feature combination (Section III). Finally, and as a relevant contribution from this work, these non-parametric classifiers were tested for the classification of impervious surfaces using two strategies: 1) a binary classification where pervious/impervious objects were directly classified; and 2) by defining and classifying subclasses (roads, rooftops, etc.) which were later on aggregated into the corresponding final pervious/impervious classes. Summing up, this study tried to find out the most appropriate combination of non-parametric classification method, feature set, and strategy in order to target pervious and impervious areas on RGB archival aerial orthoimages (which had poor radiometry and many artefacts due to poorly-preserved positives).

II. Study Area and Data Sets

The study area comprised of a rolling terrain and the heavily developed coastal fringe of Almería (Mediterranean coast, Southern Spain), approximately 11,000 m long and 775 m wide. The target area was situated between the harbors of Garrucha and Villaricos (Fig. 1). This area has suffered from a significant and persistent sealing process since the mid-1960s due to urban development, derived from touristic activities, which has led to an increase in impervious surfaces in this area.

The classification approaches tested in this work were applied to the archival RGB aerial orthoimages obtained from a photogrammetric flight carried out on April 9, 2001. The original photographs were acquired by the Coastal Board (Spanish Government) by using a RC30 ($\text{focal distance} = 152.92\ \text{mm}$) analogical camera at an approximate scale of 1:5000. The relatively poorly-preserved positives which had poor radiometry and many artefacts (scratches, fingerprints, etc.) were digitized by a photogrammetric scanner resulting in a Ground Sample Distance (GSD) close to 0.10 m, with a resolution of 20 μm in the RGB channels (8 bits). The final RGB orthoimages were obtained through a standard digital photogrammetry process carried out with the software SOCET SET©, and the final spatial resolution, or GSD, was 0.20 m.

A high spatial variability in the radiometric values was detected. In fact, atmospheric haze variations, poor conservation of the original positives and, mainly, the so-called "hot-spot" effect, which makes most landscapes appear brighter when the viewing direction in the image gets closer to the lighting direction of the sun, are well-known sources of radiometric heterogeneities in aerial images [33]. Thus, since the orthoimagery was obtained from different aerial images which were radiometrically heterogeneous, the resulting orthoimages showed areas with different radiometry. It should be noted that a radiometric correction was not carried out on the images. This was not done so that the original digital numbers were preserved and because the input data required to perform an atmospheric correction were not available, which happens for most of the aerial archival

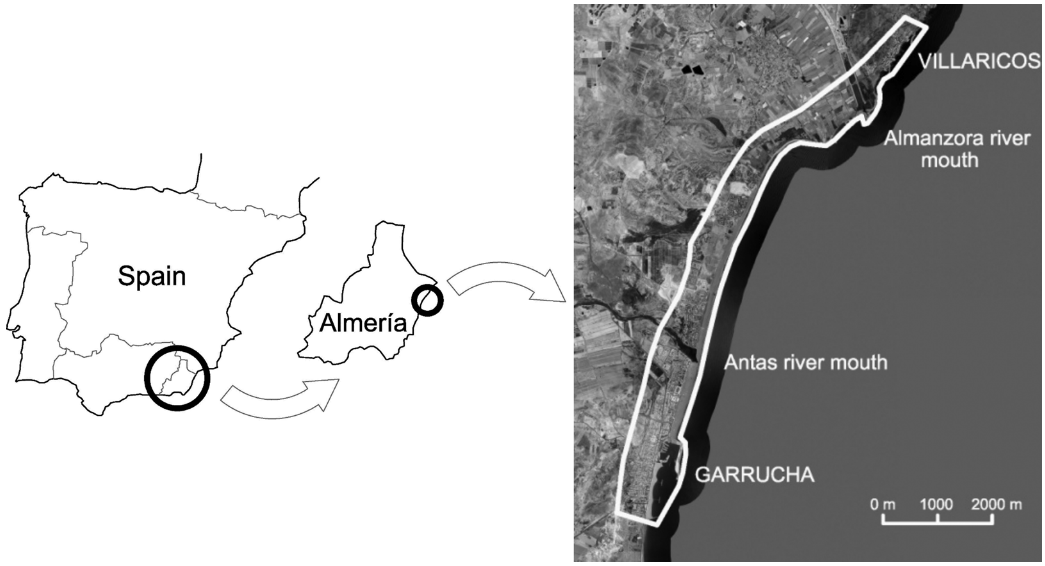

Fig. 1. Location of the study site on the Almeria coast, Southeastern Spain.

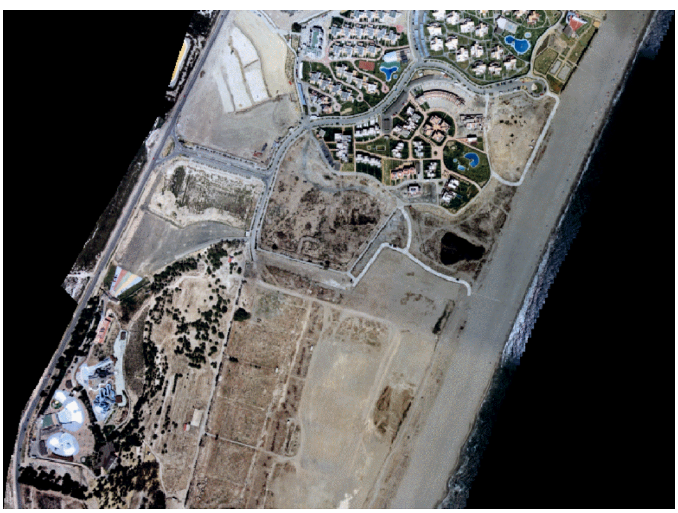

Fig. 2. Orthoimage corresponding to the central area of the study site.

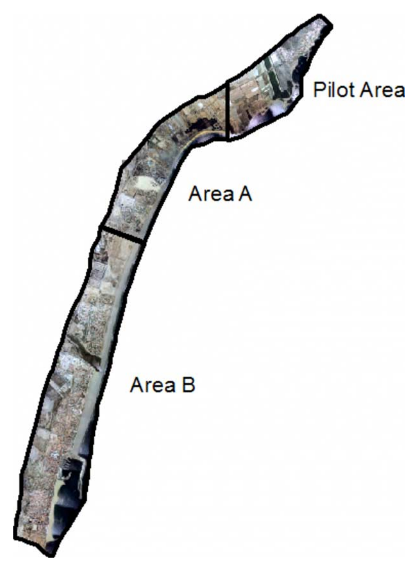

Fig. 3. Distribution of the three study areas.

data [33]. Moreover, relative or absolute atmospheric corrections were not required [34], since the main goal of this work was not to estimate biophysical variables (where radiance and reflectance are needed), but to classify pervious and impervious areas using the digital numbers from the RGB bands as input. In order to take into account the radiometric heterogeneity, two radiometrically different areas (North and South) were identified in the study area, as shown in Fig. 2. This kind of radiometrical irregularity is a common drawback of mosaicked archival or historical images, and suggests that the introduction of radiometrically independent features, (e.g., RGB ratios and texture indices) can be suitable for image classification [35], [36]. In order to overcome the radiometric artefact, the classification process should be independently applied to each of the radiometrically homogeneous areas, thus the study area was divided into two data sets.

Although the main goal was to find a suitable approach for the entire study area, a pilot area was first selected in order to carry out the initial tests. The pilot area that was chosen was located in the northern part of the image since it had a good representation of most of the land uses that were in the whole study area (e.g., sea, urban, agricultural, forest). The size of the pilot area was 162.5 ha, covering around 25% of the total area. The final workflow obtained from the pilot area was eventually tested on the entire image. The rest of the study area was divided in two additional regions because of the previously mentioned radiometric discontinuity. Thus, the northern part of the study area (pilot area was not included) was identified as area A, and the southern part as area B (Fig. 3). In order to validate the classification method, the spatial distribution of the target classes had to be taken into account. In this sense, the pilot area had a class distribution similar to the class distribution in area B (large percentage of urban area), while the non-urban class was the predominate class in area A.

TABLE I
TARGET CLASSES AND CORRESPONDING SUBCLASSES. NUMBER OF TRAINING AND VALIDATION SAMPLES USED FOR THE CLASSIFICATION AND ACCURACY ASSESSMENT OF THE PILOT AREA.

Subclass	Target class	Number of Training samples	Number of Validation samples	Total number of Validation samples	Total number of Training samples
Dark sea	Pervious	23	35	455	143
Bright sea		23	31		
Individual trees		16	29		
Bare soil		20	72		
Scrubland		18	71		
Beach		20	68		
Cultivated agricultural field		9	67		
Non-cultivated agricultural field		4	31		
Forest		10	51		
Red building	Impervious	20	41	284	71
White building		6	28		
Gray building		4	19		
Road		13	51		
Path		8	24		
Harbour dam		2	22		
Sports court		1	5		
Swimming Pool		2	9		
Greenhouse		10	61		
Sidewalk		5	24		
Total sample size		214	739	739	214

III. METHODS

A. Minimum Classification Unit

The analysis carried out in this study was based on the OBIA approach, so the object (a set of pixels which are homogeneous regarding certain features) constitutes the minimum classification unit and also the unit used for validation purposes. The segmentation algorithm used was the multiresolution segmentation [23] implemented in eCognition 8. This approach requires the following input data: 1) quantitative information (e.g., spectral bands) used for the segmentation and its weight on the process; and 2) scale, shape and compactness parameters. For a comprehensive explanation of the algorithm and parameters see [23]. In the present study, the segmentation was carried out using the RGB digital numbers as inputs (same weight), a scale parameter of 50, and shape and compactness parameters of 0.3 and 0.7, respectively. The final values of the parameters were fixed after several tests, in order to select the combination of final segments which fit the actual field plots the best.

B. Classes to Extract and Classification Strategies

The aim of this work was to classify pervious and ISA, which were identified as *target classes*. These two classes were not defined by their own spectral characteristics, so they were defined by spectrally homogenous land cover (*subclasses*), which were classified and added to the target classes according to their perviousness/imperviousness. A classification method which tried to identify each visually recognizable class was proposed and those classes were additionally aggregated according to their perviousness as a pervious or an impervious class. The description of the subclasses and the target class that they belong to are shown in Table I.

Regarding the classification strategies workflow, two main approaches were carried out. The first one, which was called *Aggregation*, involved two steps: 1) classification of each subclass (land cover) using the different classification approaches; and 2) aggregation of each subclass to its corresponding target class, so the final classes were *Pervious* and *Impervious*. The second classification method was called *Direct Classification*, since the subclasses were not identified separately, and the two target classes were directly obtained by using the training samples corresponding to the land cover that was assigned to each target class. The aims of testing different classification strategies were to find out if there was any impact in the accuracy of the classification and if the impact depended on the considered algorithm. Choosing the most suitable strategy could result in minimizing the effort to identify the training data required for the classification [37].

C. Features Tested for Image Classification

Since the classification was based on image objects, the applied features were calculated for each object according to the pixels that formed the object. Each object was therefore characterized by using the RGB information. Unfortunately, valuable information commonly used in this sort of studies such as LiDAR data, GIS ancillary data, or vegetation indices which use the infrared part of the spectrum (e.g., Normalized Digital Vegetation Index (NDVI) or Soil-Adjusted Vegetation Index (SAVI)) were not available for their application. Nevertheless, additional features were calculated and used in the analysis. First, a simple set of ratios were derived from the original RGB bands in order to evaluate their potential as input features for the classification process. The computed features were: the green ratio ($\mathrm{G}/(\mathrm{R}+\mathrm{G}+\mathrm{B})$), the red ratio ($\mathrm{R}/(\mathrm{R}+\mathrm{G}+\mathrm{B})$), the blue ratio ($\mathrm{B}/(\mathrm{R}+\mathrm{G}+\mathrm{B})$) and the green-red ratio (G/R). The green, red and blue ratios are three chromaticity color transformations which provide additional spectral information. These transformations are useful for images were data are strongly correlated (e.g., RGB images, since correlations between blue, green and red digital numbers are often larger than 0.9), because they decorrelate the image so that the weakly correlated components of the data (i.e., the chromatic information) can be enhanced independent of the correlated intensity component [38]. The use of the green-red ratio is based on the three groups of spectral patterns for major components of land cover which can be found by using the information provided by the green and red regions of the spectrum [39]. Thus, in the case of green vegetation, green reflectance is higher than red reflectance (i.e., $\mathrm{G}/\mathrm{R} > 1$, expressed in digital numbers for archival aerial photographs), while for roofs or concrete, green reflectance is lower than red reflectance (i.e., $\mathrm{G}/\mathrm{R} < 1$). Regarding water or snow, green and red reflectance are similar (i.e., $\mathrm{G}/\mathrm{R} = 1$). Therefore the G/R index can be used as a surrogate of red-infrared ratio (R/IR) to distinguish vegetation from other land cover, and to differentiate types of vegetation [40]. Moreover, the use of band ratio images that include short wavelength bands has been proved to be effective for lithological mapping [41], since they contribute to suppress the topographic variation and the brightness difference related to grain size variation.

Moreover, texture features (e.g., variance) have been found to be essential in order to provide better results when very high spatial resolution orthoimages are used [42]. Texture features are considered to be more suitable than absolute radiometric values which can vary artificially along the entire data set, particularly when working with archival imagery (see Fig. 2). Finding the most suitable texture indicator was beyond the scope of this work (for more information about finding the most suitable texture indicator please refer to [43] and [44]), so only two widely used texture measurements were tested. The first one was the local variance, which was computed using a 7×7 window size [45] using the formula:

$$Variance = \sum_{i=1}^{n} \frac{\left(DN_{x,y} - \overline{DN}\right)^2}{n-1} \qquad (1)$$

where $DN_{x,y}$ represents the digital number of the pixel located at row x and column y and $\overline{DN}$ being the mean digital number for the $\mathrm{n} = 49$ pixels that belong to the mobile window.

The window size was considered large enough to satisfactorily capture the textural patterns of the objects according to the land-use class that needed to be identified. The local variance was computed for each RGB band as a raster image and added to the feature space, so that the mean and the standard deviation could be calculated for each object.

The second type of texture feature was based on the Gray Level Co-occurrence Matrix ("GLCM") descriptors available in eCognition, i.e., an object-based version of the original features proposed by [46]. Among all of the available features, homogeneity and correlation were chosen since they have been tested and recommended by different authors. [47] and [48] pointed out that homogeneity is the most suitable texture measurement that can be used to differentiate urban land uses, while correlation was suggested by [48] and [49] as one of the most suitable "GLCM" statistics. Furthermore, homogeneity and correlation are not linear dependent features [50].

The computed features were grouped into different subsets or feature vectors (Table II) in order to know the impact of the different features on the classifiers, as well as their performance for the whole classification process. Thus, the feature vector called "Basic" grouped the RBG bands into derived features including the mean value of each band and the four band ratios as previously described. The "Basic" feature vector including the band ratios was preferred over the simple RGB feature vector after comparing the results of using each one as input data. It was found that using the "Basic" feature provided a significantly better classification (overall accuracy and Kappa) for two of the three classification methods that were tested (i.e., CART, NN), while for the other classifier (SVM) the differences were not statistically significant at a 95% confidence level.

The group "Variance" was comprised of all the "Basic" features plus the mean and standard deviation of the local variance texture, which was estimated according to (1). The "GLCM" group had the "Basic" features plus the "GLCM" texture features used in this work. All the previously mentioned features were included in the feature vector called "Total", which resulted in a vector which was defined by 19 features.

D. Non-Parametric Classification Methods Tested

Classification and Regression Tree (CART) analysis was the first tested method. CART is a non-parametric method widely used in remote sensing for image classification [49], [51], and [52]. The most explanatory variables are detected by this kind of analysis and a prediction of response values can be carried out. CARTs use a sequential method for class assignment issues in which tree construction requires a recursive partitioning of the training data set, which is divided into subsets, increasing their internal homogeneity according to one or more features [53]. The decision tree model that was used in this work corresponded to the univariate CART described by [54], with no pruning algorithm being applied [55].

The Nearest Neighbor (NN) method was the second tested method. NN is a non-parametric supervised classification approach which stands out because of its simplicity and flexibility [32], [56]. It is characterized by achieving suitable results when the number of required training samples is not very high [57]. The k nearest neighbors in the feature space are searched for in order to determine which class the element being classified belongs to. Although k-NN methods benefit the outlier effect removal, they also involve a large computational effort [58]. However, OBIA approaches enable k-NN methods to be applied in a more efficient way, since the use of objects can significantly reduce the number of elements that need to be classified, when compared to using pixels as minimum classification unit [59]. In this work, the 1-NN approach was used [60] as implemented in

TABLE II
FEATURE VECTORS.

"Basic"	"Variance"	"GLCM"	"Total"
Mean Red			
Mean Green			
Mean Blue	Basic	Basic	Basic
Green Ratio			
Red Ratio	+	+	+
Blue Ratio			
Green-Red Ratio			
7 features	Mean Variance Red	Homogeneity Red	Mean Variance Red
	Mean Variance Green	Homogeneity Green	Mean Variance Green
	Mean Variance Blue	Homogeneity Blue	Mean Variance Blue
	Std. dev. Variance Red	Correlation Red	Std. dev. Variance Red
	Std. dev. Variance Green	Correlation Green	Std. dev. Variance Green
	Std. dev. Variance Blue	Correlation Blue	Std. dev. Variance Blue
	13 features	13 features	Homogeneity Red
			Homogeneity Green
			Homogeneity Blue
			Correlation Red
			Correlation Green
			Correlation Blue
			19 features

the eCognition software. This approach allows the membership probability value of every object belonging to each target class to be computed [51], [57] according to the description in [61].

The third method that was tested was Support Vector Machine (SVM), which is a non-parametric supervised learning technique used for classification and regression analysis. The application of SVM on remote sensing image classifications has increased extraordinary recently mainly because: 1) it does not rely on the assumption that the data are drawn from a given probability distribution; and 2) it requires a relative small number of training samples [30], [62], which is an advantage due to the difficulty in obtaining ground truth samples. SVM has been previously used for impervious surface mapping or urban area classification [63], [64] using hyperspectral data [65] or high resolution satellite imagery [66]. However, few applications have been carried out on archival aerial RGB photography [67]. Therefore the successful application of an object-based classification using SVM on the dataset used in this work could boost the use of these techniques for long-term land-use evolution studies.

In short, SVM methods try to find a hyperplane which splits a data set into two subsets during the training phase, using a set of samples where the classification is previously known [68]. The training phase tries to find the optimum boundary decision solution that minimizes misclassifications [30]. A crucial aspect of SVM is that not all samples are used to define the final hyperplane. Only those samples which are in the margin between classes are used to define the hyperplane and they are called Support Vectors [64]. To obtain that hyperplane, a kernel function needs to be used. The radial basic function (RBF) is the most commonly used approach and therefore it was used, following the formula expressed in the equation [69], [70]:

$$K\left(x_i, x_j\right) = e^{-\gamma\left(x_i - x_j\right)^2}; \gamma > 0 \tag{2}$$

where the kernel parameter γ, together with the penalty parameter of the error term (usually denoted by C, with $\mathrm{C} > 0$) are estimated from the training data set through cross validation [69].

In the present work, the free-distribution library LIBSVM [69] was used for the application of SVM classifier. The general methodology proposed by the authors was also applied. This methodology consists of the following steps: 1) a simple scaling is applied to the training data (in order to avoid the over-weighting due to the features presenting the highest absolute values); 2) the applied kernel is RBF. The determination of parameters C and γ is solved by cross validation and grid search on the training data set. Then, 3) the estimated parameters are applied to the dataset used for testing (previously scaled), and the error matrix is computed. Finally, 4) the computed SVM parameters are applied to the set of objects that are within the entire image.

Each non-parametric classifier previously described (CART, NN and SVM) was applied, using as an input each of the four feature vectors ("Basic", "Variance", "GLCM" and "Total"). Both classification strategies (i.e., *Aggregation* and *Direct Classification*) were carried out for each combination of classifier and feature vector, which led to 24 different classifications being undertaken (3 classifiers $\times$ 4 feature vectors $\times$ 2 strategies). However, taking into account the description of NN approach, it has to be clarified that both strategies have been proved to achieve the same classification results since the nearest sample in the feature space will be the same for both strategies, e.g., if the nearest sample corresponds to "Forest" for the *Aggregation* strategy, it will necessarily correspond to "Pervious" for the *Direct Classification*. Thus, the number of combinations is reduced to 20 final classifications.

E. Validation and Comparison

The sampling design, both for the training stage and the accuracy assessment, is a crucial task in the image classification process. Since the homogeneous object was established as the minimum classification unit in this work, they were also chosen as the unit used for the training and testing samples, instead of using single pixels. A randomly stratified sampling method was followed, so that well distributed random samples were identified for each subclass. The samples were located on the orthoimages and each sample was assigned to the corresponding subclass (Table I). The high spatial resolution of the orthoimages enabled each class to be identified visually with no detectable errors.

It has been widely proven in previous works that classification accuracy can be affected by training sample size [70]–[72]. It is also known that the number of required samples depends on both the classifier [71] and the number of classes to be labelled [70]. On the other hand, the number of validation samples that are needed to carry out the accuracy assessment needs to be larger than the training dataset in order to achieve narrow confidence intervals for the accuracy estimation. [73] suggested that 50 could be a proper number of samples per class when the scene is not too extensive, while a number from 75 to 100 would be advisable for vast areas or predominant classes. Otherwise, some statistically-based formulas such as binomial distribution [74] or multinomial distribution [75] are suggested. These methods utilize the expected precision per cent and the toleration error in order to estimate the testing sample size. According to [75], the validation sample size for the pilot area (739, see Table I) can be considered suitable, and slightly higher than necessary to achieve an overall accuracy of 85% ($p < 0.05$).

Error matrices were calculated for each classification and overall accuracy (OA), user's accuracy (UA), producer's accuracy (PA) and KHAT statistic were derived [73]. Additionally, in order to offer significance to the given results, intervals of confidence by Exact method [76] were calculated ($p < 0.05$), because it corresponds to the maximum likelihood estimate (i.e., the actual value of the estimated accuracy OA, UA or PA) even when it is not symmetrical (the values above and below are reported). The result of performing a Kappa analysis is a KHAT statistic ($\widehat{K}$), an estimate of Kappa. Additionally, the variance of $\widehat{K}$, and the Z statistic can be calculated to test the significance of a single error matrix (see [75] for further information). The Kappa test was applied [75] at a statistical level of significance $p < 0.05$, in order to estimate whether the error matrix was statistically different from another one. In order to compare two independent error matrices (i.e., 1 and 2), the following statistic is calculated:

$$Z_{12} = \frac{\left|\widehat{K_1} - \widehat{K_2}\right|}{\sqrt{\widehat{var}(\widehat{K_1}) + \widehat{var}(\widehat{K_2})}}. \tag{3}$$

This statistic is also standardized and normally distributed. Thus, the null hypothesis ($K1 - K2 = 0$) will be rejected if $Z \geq 1.96$ ($p < 0.05$). That rejection would mean that the error matrices 1 and 2 are considered significantly different at a 95% confidence level.

190 different comparisons between methods were made by applying the Kappa test. In order to help understand the results, a separability matrix (SM) was computed (see Section IV). The matrix was defined by the statistics used to compare the different classification approaches, so the statistics given by (3) were calculated for each approach versus the other 19 approaches.

IV. Results and Discussion

As previously mentioned, the main goal of this paper was to address three issues: (i) what non-parametric classifier yielded the most accurate output; (ii) what feature set led to the most accurate classification and; (iii) if the application of *Aggregation* or *Direct Classification* strategies affected the accuracy. On one hand, this section shows and discusses the accuracy values obtained by each approach and the statistical comparison between the different approaches (Section IV-A), to determine if they were statistically different. On the other hand, once the most accurate method was selected, this section establishes a protocol (Section IV-B) and tests it in an operational context (Section IV-C).

A. Accuracy Assessment Results and Comparisons

A summary of the results of the accuracy assessment, showed as the 95% confidence intervals, are presented in Table III for each target class. The highest overall accuracy was achieved with the SVM and NN approaches in those cases in which "Total" or "Variance" feature vectors were used, i.e., when the local variance texture feature was included. Those results were considered to be suitable since the OA was higher than 85%, which has been established as the minimum acceptable value for the classification results by [75]. That minimum seemed to be a reasonable reference for the required accuracy in this work, since there was a large variability within the classes that were labelled and the radiometric quality of the archival data set was relatively poor. The results obtained in our work could be considered more accurate than those in previous work with basic comparative information (no infrared band and high spatial resolution) which achieved an OA of around 80% for ISA detection [27]. Another comparable study carried out by [16] achieved an OA of 90% with a high spatial resolution Quickbird image, which included the near-infrared band. [2] obtained an OA of 81% for urban classification with digital 1-m spatial resolution orthoimagery. On the other hand, the CART approaches provided the lowest classification accuracies. Regarding the Producer's accuracy (PA), it was systematically higher for the pervious class than for the impervious class, which meant that the impervious objects had a larger omission error than the pervious objects, especially for the CART approaches. Generally, the same occurred for the User's accuracy (UA). As a result, it can be said that the pervious class was better classified than the impervious class, being more noticeable in the case of the PA results. Taking into account that the sample design was balanced (33% of classified objects were impervious while the 37% of validation and training samples were from the same target class), the differences between the results of impervious and pervious classes happened because objects in impervious class were made by different kinds of construction materials, which leads to a spectrally heterogeneous class [77]. In order to prove the latter, the error matrix corresponding to the subclasses was computed (not shown). As an example, the classification of impervious subclasses such as roads, paths and harbor dam

TABLE III
CONFIDENCE INTERVAL OF ACCURACY ASSESSMENT RESULTS FROM THE CORRESPONDING ERROR MATRICES. THE FEATURE VECTORS ARE DENOTED AS *BASIC* (B), *GLCM* (G), *VARIANCE* (V) AND TOTAL(T), WHILE THE CLASSIFICATION STRATEGIES ARE CODED AS *AGGREGATION* (1) AND DIRECT CLASSIFICATION (2).

	Overall accuracy	Producer's Accuracy		User's Accuracy	
		Pervious	Impervious	Pervious	Impervious
CART_B_1	77.8 - 83.6	87.5 - 93.1	59.3 - 70.7	76.9 - 84.0	75.5 - 86.0
CART_B_2	69.2 - 75.7	79.6 - 86.6	49.3 - 61.2	70.9 - 78.6	61.0 - 73.4
CART_G_1	75.6 - 81.7	91.7 - 96.2	47.9 - 59.8	72.9 - 80.1	79.5 - 90.3
CART_G_2	69.0 - 75.6	82.9 - 89.4	44.0 - 56.0	69.5 - 77.2	62.8 - 75.8
CART_V_1	78.2 - 84.0	78.6 - 85.8	74.0 - 83.8	82.8 - 89.5	68.5 - 78.6
CART_V_2	72.9 - 79.2	89.2 - 94.4	44.7 - 56.7	71.2 - 78.5	73.4 - 85.6
CART_T_1	78.2 - 84.0	80.5 - 87.4	71.0 - 81.2	81.5 - 88.3	69.7 - 80.0
CART_T_2	71.4 - 77.8	76.3 - 83.8	60.0 - 71.4	75.0 - 82.6	61.7 - 73.0
NN_B	82.8 - 88.0	85.0 - 91.2	75.9 - 85.4	84.8 - 91.0	76.2 - 85.7
NN_G	78.9 - 84.6	82.4 - 89.0	69.9 - 80.3	81.4 - 88.1	71.6 - 81.8
NN_V	83.6 - 88.7	84.6 - 90.8	79.0 - 87.9	86.5 - 92.4	76.3 - 85.5
NN_T	85.2 - 90.1	87.7 - 93.3	78.2 - 87.3	86.4 - 92.2	80.1 - 88.9
SVM_B_1	77.9 - 83.7	87.0 - 92.7	60.4 - 71.7	77.3 - 84.4	75.0 - 85.6
SVM_B_2	76.9 - 82.8	89.5 - 94.6	54.3 - 66.0	75.1 - 82.2	77.2 - 87.9
SVM_G_1	78.8 - 84.5	83.1 - 89.6	68.4 - 79.0	80.6 - 87.4	72.1 - 82.3
SVM_G_2	78.2 - 84.0	84.6 - 90.8	64.7 - 75.7	79.0 - 85.9	72.9 - 83.3
SVM_V_1	85.1 - 90.0	85.0 - 91.2	82.1 - 90.4	88.3 - 93.8	77.5 - 86.4
SVM_V_2	87.0 - 91.6	89.5 - 94.6	80.2 - 88.8	87.7 - 93.2	82.8 - 91.0
SVM_T_1	86.1 - 90.8	87.2 - 92.9	81.3 - 89.7	88.1 - 93.6	80.0 - 88.7
SVM_T_2	86.9 - 91.4	89.0 - 94.2	80.5 - 89.1	87.9 - 93.3	82.2 - 90.5

yielded, respectively, an omission error of 23.53%, 33.33% and 59.09% with the pervious subclasses. Note that SVM with the feature sets "Variance" and "Total" and NN with all feature sets, presented very similar values of PA and UA for both target classes, while SVM with the feature sets "Basic" and "GLCM" and especially CART with all the feature sets, yielded larger differences between PA and UA.

As a measure of agreement or accuracy, KHAT is considered to show strong agreement when it is greater than 0.75 [78], while values lower than 0.40 indicate poor agreement [75]. According to Table IV, the SVM approach with the "Variance" and "Total" feature vectors and NN with "Total" could be considered results that have strong agreement. However, the CART approaches were showed to be the least accurate, especially when the direct classification approach was applied, since the internal heterogeneity [77] made it difficult to achieve a suitable separation using regression trees. Thus, the CART classifier was capable of identifying the most explanatory variables that were needed to classify the most abundant subclasses, increasing the internal homogeneity and improving the final overall accuracy when the *Aggregation* strategy was applied. Noticeably, those subclasses (i.e., dark sea, bright sea or individual trees as pervious classes, and red buildings or greenhouses as impervious surfaces) had the largest weights over the entire scene. On the contrary, when only two highly heterogeneous subclasses were considered, i.e., pervious and impervious, the variables which improved the homogeneity were not as easy to obtain and consequently, the accuracy achieved was significantly lower for *Direct Classification* strategy.

In order to determine the influence of the two different classification strategies (*Aggregation* and *Direct Classification*) as well as to carry out a statistical comparison between the two methods, KHAT values were computed both for all the error matrices and for each target class, pervious and impervious. The results shown in Table IV, pointed out that only the CART approaches with all feature vectors were significantly affected ($p < 0.05$) by the classification strategy. Otherwise, from the results of SVM approaches can be inferred that the classification agreement was not statistically sensitive to the use of subclass aggregation or the application of a direct binary classification. It should be noted that only when pervious subclasses were confused with impervious ones (and vice versa) (e.g., bare soil was misclassified as roads or paths, and roads were misclassified as scrubland), the accuracy results were affected. Therefore, although some subclasses were difficult to classify, the most common misclassifications were commonly with other subclasses of the same target class (e.g., scrubland was misclassified mostly with agricultural fields) so the final accuracy was not affected. It is relevant to highlight that, since the training samples were acquired through a balanced random stratified sampling for each subclass, most of the spectral variability of the final target classes were successfully captured from the subclass-based training. Only when this kind of sampling is carried out—extracting samples from every significant subclass, a successful classification of the target classes can be expected. Otherwise, the expected results when using the direct classification approach could be different.

TABLE IV
KHAT STATISTIC FOR EACH COMBINATION OF CLASSIFIER, FEATURE VECTORS AND CLASSIFICATION STRATEGY AND Z STATISTIC CORRESPONDING TO THE DIFFERENCES BETWEEN THE TWO TESTED CLASSIFICATION STRATEGIES REGARDING OVERALL ACCURACY. SIGNIFICANT DIFFERENCES ($p < 0.05$) IN CLASSIFICATION OVERALL ACCURACY ARE HIGHLIGHTED IN BOLD LETTERS.

Approach	KHAT (overall accuracy)	Z statistic for the two different classification strategies
CART_B_1	0.5783	**3.8268**
CART_B_2	0.3993	
CART_G_1	0.5175	**2.8617**
CART_G_2	0.3841	
CART_V_1	0.6080	**2.6774**
CART_V_2	0.4816	
CART_T_1	0.6038	**3.2650**
CART_T_2	0.4628	
SVM_B_1	0.5827	0.7736
SVM_B_2	0.5538	
SVM_G_1	0.6106	0.4405
SVM_G_2	0.5948	
SVM_V_1	0.7423	0.7656
SVM_V_2	0.7758	
SVM_T_1	0.7604	0.2919
SVM_T_2	0.7734	
NN_B	0.6938	Not applicable
NN_G	0.6190	Not applicable
NN_V	0.7129	Not applicable
NN_T	0.7416	Not applicable

In order to determine the most adequate combination of classifier, feature set and strategy, several separability matrices (SMs) were used (see Tables V–VIII). A SM depicts every approach to be compared in columns and rows from the highest KHAT to the lowest one so that the same order is followed. Every cell of the matrix represents the Z statistics (3) between each pair of approaches so the diagonal cells correspond to the same method and therefore the Z statistic for those cells is zero. Therefore, the SM is a valuable tool that can easily identify which methods are significantly different from the others. In this work, since the total size of the SM for all the approaches (20×20 dimension) did not allow a proper display, the results are shown in order to independently analyze the influence of every studied variable, i.e., classification strategy, classifier and feature vector.

Table V shows the separability for all the approaches which used the *Direct Classification*. The SVM and NN classifiers in combination with the feature sets "Variance" and "Total" yielded the best accuracy results and they were significantly different from the other approaches (although NN with the feature set "Basic" was not separable from the NN "Total" and "Variance"). Similar results were found in the SM of *Aggregation* strategy approaches. Those results implied that the "GLCM" feature set was not able to achieve any similar results regarding the accuracy of the classification and did not add any relevant information for the classification of ISA in this study area. This was probably due to the fact that the GLCM matrices were computed within each object and homogeneity and correlation were estimated for each independent object (OBIA approach). Instead, the texture obtained as local variance has been proved to have a large influence on the improvement of accuracy, probably due to the independence of the object limits and the window size which is large enough to extract a suitable spectral variability [42]. Moreover, the CART approaches were clearly pointed out as the least accurate classifiers.

In order to clarify the impact of the different approaches on each classifier, a SM comprising of all the approaches that used the same classifier was computed. Table VI shows the SM for the SVM classifier and highlights two aspects: first, non-significant differences existed between the feature sets "Variance" and "Total" and second, no differences were detected among approaches which used "GLCM" and "Basic" feature sets either. However, both blocks (i.e., "Variance" and "Total" vs. "GLCM" and "Basic") were clearly distinguished, highlighting that "Variance" and "Total" feature sets yielded the most accurate results for the SVM classifier. Similar results were found for NN but the "Basic" feature set did not achieve significant differences from "Variance" or "Total" showing that NN was less dependent on the chosen feature set (Table VII). Regarding CART, the strategy used was the main factor that affected its accuracy, the *Aggregation* strategy being the most accurate. The feature sets played a less important role for the CART classifier.

Finally, a SM of all the approaches that used the same feature set was displayed. Table VIII shows all the combinations with the "Total" feature set. It can be pointed out that only CART can be considered as the least accurate classifier, since its KHAT statistics were significantly different from all of the other approaches (the highest KHAT for CART was 0.6038, while for the other approaches the KHAT values were between 0.7416 and 0.7733). Additionally, the type of strategy employed had no influence on the approach except for the CART classifier. Similar behavior was observed for the "Variance" and "GLCM" feature sets. However, when the "Basic" feature set was applied, the NN resulted to be significantly more accurate than the other classifiers and SVM and CART were similar when CART was applied to the *Aggregation* strategy.

Therefore, according to the results previously discussed it can be proved that: (i) the most accurate classifiers were NN and SVM, (ii) NN was the least dependent classifier on the feature set employed, (iii) only CART was dependent on the strategy that was followed; and (iv), the feature sets which allowed the most accurate results to be obtained were "Total" and "Variance". As a result, the CART classifier could have been rejected as an accurate classifier for this study while it has been proved that the incorporation of the texture variance was significant in order to increase the accuracy of the ISA classification using archival RGB images.

B. *Establishment of an Operational Protocol*

From both operational and mapping production standpoints, the efficiency of the classification process is crucial for the selection of the final approach. In that sense, the SVM classifier was highlighted as being clearly more efficient than the NN classifier. Table IX shows a comparison of the computational budget (measured as running time) needed in order to carry out the ISA classification for the pilot area. The measured time

TABLE V
SEPARABILITY MATRIX FOR CLASSIFICATION STRATEGY 2 (DIRECT CLASSIFICATION). BOLD TYPE INDICATES SIGNIFICANT DIFFERENCES ($p < 0.05$).

	SVM_V_2	SVM_T_2	NN_T	NN_V	NN_B	NN_G	SVM_G_2	SVM_B_2	CART_V_2	CART_T_2	CART_B_2	CART_G_2
SVM_V_2	0	0.071	0.956	1.644	**2.069**	**4.400**	**4.653**	**5.601**	**7.643**	**7.904**	**9.420**	**10.244**
SVM_T_2	0.071	0	0.887	1.578	**2.005**	**4.326**	**4.584**	**5.532**	**7.568**	**7.832**	**9.347**	**10.165**
NN_T	0.956	0.887	0	0.720	1.161	**3.304**	**3.627**	**4.559**	**6.484**	**6.774**	**8.245**	**8.971**
NN_V	1.644	1.578	0.720	0	0.440	**2.398**	**2.764**	**3.665**	**5.459**	**5.765**	**7.173**	**7.802**
NN_B	**2.069**	**2.005**	1.161	0.440	0	1.867	**2.254**	**3.140**	**4.868**	**5.183**	**6.559**	**7.142**
NN_G	**4.400**	**4.326**	**3.304**	**2.398**	1.867	0	0.517	1.491	**3.307**	**3.674**	**5.154**	**5.740**
SVM_G_2	**4.653**	**4.584**	**3.627**	**2.764**	**2.254**	0.517	0	0.932	**2.634**	**3.002**	**4.413**	**4.929**
SVM_B_2	**5.601**	**5.532**	**4.559**	**3.665**	**3.140**	1.491	0.932	0	1.655	**2.039**	**3.438**	**3.909**
CART_V_2	**7.643**	**7.568**	**6.484**	**5.459**	**4.868**	**3.307**	**2.634**	1.655	0	0.431	1.873	**2.301**
CART_T_2	**7.904**	**7.832**	**6.774**	**5.765**	**5.183**	**3.674**	**3.002**	**2.039**	0.431	0	1.415	1.815
CART_B_2	**9.420**	**9.347**	**8.245**	**7.173**	**6.559**	**5.154**	**4.413**	**3.438**	1.873	1.415	0	0.347
CART_G_2	**10.244**	**10.165**	**8.971**	**7.802**	**7.142**	**5.740**	**4.929**	**3.909**	**2.301**	1.815	0.347	0

TABLE VI
SEPARABILITY MATRIX FOR SVM CLASSIFIER. BOLD TYPE INDICATES SIGNIFICANT DIFFERENCES ($p < 0.05$).

	SVM_V_2	SVM_T_2	SVM_T_1	SVM_V_1	SVM_G_1	SVM_G_2	SVM_B_1	SVM_B_2
SVM_V_2	0	0.071	0.447	0.961	**4.292**	**4.653**	**4.927**	**5.601**
SVM_T_2	0.071	0	0.376	0.889	**4.223**	**4.584**	**4.859**	**5.532**
SVM_T_1	0.447	0.376	0	0.514	**3.856**	**4.218**	**4.493**	**5.167**
SVM_V_1	0.961	0.889	0.514	0	**3.354**	**3.718**	**3.994**	**4.666**
SVM_G_1	**4.292**	**4.223**	**3.856**	**3.354**	0	0.369	0.645	1.303
SVM_G_2	**4.653**	**4.584**	**4.218**	**3.718**	0.369	0	0.276	0.932
SVM_B_1	**4.927**	**4.859**	**4.493**	**3.994**	0.645	0.276	0	0.655
SVM_B_2	**5.601**	**5.532**	**5.167**	**4.666**	1.303	0.932	0.655	0

TABLE VII
SEPARABILITY MATRIX FOR NN CLASSIFIER. BOLD TYPE INDICATES SIGNIFICANT DIFFERENCES ($p < 0.05$).

	NN_T	NN_V	NN_B	NN_GLCM
NN_T	0	0.720	1.161	**3.304**
NN_V	0.720	0	0.440	**2.398**
NN_B	1.161	0.440	0	1.867
NN_GLCM	**3.304**	**2.398**	1.867	0

was exclusively referred to as the classification task, excluding the previous segmentation phase. When using the NN classifier both the number of classes to be classified and, especially, the feature vector, had an influence on the running time for computing the classification results. The computational cost of processing the feature vectors including the texture indices based on "GLCM" (homogeneity and correlation) turned out to be actually unaffordable under real operational conditions for current mapping production, as it has been previously indicated by other authors [79]–[81]. Comparatively, the texture index, based on local variance previously computed for a 7×7 window size, took less than five minutes of additional running time than when the "Basic" feature vector was used. As a result, the use of the "GLCM" texture was not efficient, especially taking into account that the pilot area comprised of only around 25% of the entire working area. Furthermore, the number of target subclasses was a key factor according to the processing time, particularly when the local variance texture was used, since the required time was fifteen times longer for the aggregation strategy than for the direct classification (17 minutes and 1 minute respectively). This fact can be explained because each object is compared to each subclass in order to be assigned to the nearest subclass. If only two classes were being compared (pervious/impervious), the process required less computational effort. The number of training samples would be another significant factor related to computational time since each element has to be compared against each object and then finally labelled according to the corresponding object. Eventually, if a NN classifier is employed, the use of a previously computed local variance texture index is suggested. In the same direction, the use of the direct classification (pervious/impervious classes) is also recommended. In that case, an exhaustive training sample is required in order to feed the classifier the whole spectral variability of the subclasses composing of the final target classes.

C. Testing the Method in an Operational Context

According to the results discussed in the previous sections, the SVM classifier is the most efficient choice when the accuracy of the results (both the producer's and user's accuracy), its low dependency on the classification strategy and, finally, its low computational budget are taken into account. Additionally,

TABLE VIII
SEPARABILITY MATRIX FOR THE APPROACHES USING THE TOTAL FEATURE VECTOR. BOLD TYPE INDICATES SIGNIFICANT DIFFERENCES ($p < 0.05$).

	SVM_T_2	SVM_T_1	NN_T	CART_T_1	CART_T_2
SVM_T_2	0	0.376	0.887	**4.105**	**7.832**
SVM_T_1	0.376	0	0.521	**3.765**	**7.448**
NN_T	0.887	0.521	0	**3.223**	**6.774**
CART_T_1	**4.105**	**3.765**	**3.223**	0	**3.063**
CART_T_2	**7.832**	**7.448**	**6.774**	3.063	0

TABLE IX
RUNNING TIME TO CARRY OUT THE PILOT AREA CLASSIFICATION USING THE NN CLASSIFIER AVAILABLE IN ECOGNITION 8, SVM, AND CART. THE RESULTS HAVE BEEN OBTAINED BY USING A 3.20 GHZ DUAL CORE PROCESSOR WITH 8 GB RAM AND 64 BITS.

Classifier	Feature vectors	Aggregation Classification Strategy (Running Time)	Direct Classification Strategy (Running Time)
NN	"Basic"	15 min 11 sec	1 min 08 sec
	"GLCM"	5 h 21 min 15 sec	4 h 22 min 21 sec
	"Variance"	16 min 50 sec	1 min 20 sec
	"Total"	6 h 50 min 02 sec	5 h 18 min 19 sec
SVM	All cases	< 1 min.	< 1 min.
CART	All cases	< 1 min.	< 1min.

TABLE X
CLASSIFICATION ACCURACY ASSESSMENT RESULTS FOR THE ENTIRE AREA BY USING THE SVM CLASSIFIER, VARIANCE FEATURE VECTOR AND DIRECT CLASSIFICATION STRATEGY.

Area	Training set	Overall Accuracy	KHAT	Z statistic	Class	Producer's Accuracy	User's Accuracy
A	Pilot area training	73.14%	0.4705	5.286	Pervious	89.16%	66.07%
					Impervious	58.70%	85.71%
	Ad hoc training	86.10%	0.7195		Pervious	79.12%	90.37%
					Impervious	92.39%	83.06%
B	Pilot area training	77.63%	0.5539	3.591	Pervious	90.49%	71.69%
					Impervious	65.06%	87.50%
	Ad hoc training	85.90%	0.7181		Pervious	86.69%	85.07%
					Impervious	85.13%	86.74%

the use of "GLCM" texture and the aggregated strategy were proved as not being significant for the accuracy improvement. Thus, the combination of the SVM method, the "Variance" feature set, and the *Direct Classification* strategy was chosen. Based on this choice, the classification of the entire working area was carried out and the results are shown in Table X. The effect of the aforementioned radiometric artefact on the classification accuracy can be observed when the results are compared. When the North and South areas (areas A and B as described in Section II) were classified using the training samples extracted from the pilot area (pilot training), the accuracy of the results were statistically poorer than when the training samples were collected from a specific area to be classified (ad hoc training in Table X). According to the Z statistic, the accuracy significantly increased for the overall accuracy and the KHAT statistic. Furthermore, the Z statistic between both ad hoc classifications showed that they were statistically similar ($Z = 0.033$) and therefore, the feasibility of the method was proved. These results highlighted the importance of the training dataset, especially when images which present radiometric artefacts (such as archival aerial orthoimages) are employed. Moreover, the subclass distribution can vary from one scene to another, which implies a different spectral variability for each specific area. According with the results, it was also found that although it improved the accuracy of the results, the use of variance-based features did not seem to contribute to the elimination of the radiometric artefact, since an *ad hoc* training set was needed for each area. Finally, it should be pointed out that the final classification results obtained from subsets A and B led to an appropriate KHAT statistic and an overall accuracy value above the minimum value of 85% as proposed by [75].

V. CONCLUSIONS

This work showed that RGB archival aerial orthoimagery can be used as a relevant data source for ISA classification, even when ancillary data are not available. However, this kind of archival imagery is usually radiometrically deficient, due to it being not well preserved (degraded from being stored improperly), scanning errors and radiometric variations among the different aerial photographs covering the working area (which can be detected when the images are mosaicked). Therefore, an adapted workflow which takes into account those characteristics was presented and validated in this work.

A relevant methodological contribution presented in this work was the exhaustive statistical analysis undertaken in order to make sure that the results that were obtained were reliable. The KHAT statistic was used to compare the error matrices corresponding to each combination (one-against-one), which indicated whether the accuracies were significantly different from one another. Because of the high number of combinations that were compared, the separability matrix (SM) was introduced as a tool to clarify the statistical analysis results. This matrix was proved to be a useful method in order to make the obtained results more intelligible and organized.

From the SMs results, some conclusions can be derived. First, SVM and NN were ranked as the most suitable classifiers, especially when the local variance texture descriptor was included in the feature vector. For those cases the overall accuracy was close to 90% and KHAT was about 0.75. Local variance represents a simple and easy way to extract texture, so its utilization and adaptation to images that have different spatial resolutions should be tested in further works. The CART classifier, based on decision trees, performed the worst regarding overall accuracy, achieving a score not higher than 82%. The absence of significant improvement regarding classification results was remarkable when texture information based on object-based "GLCM" (homogeneity and correlation texture indices) was added to the basic spectral features (mean of the RGB channels and 4 different band ratios for each object). Additionally, "GLCM"-based texture indices are computationally expensive and, therefore, difficult to implement under operational conditions or mapping production.

Another notable conclusion that can be extracted from this work is the relative low influence of the classification strategy (aggregation of subclasses or direct classification) on the pervious/impervious classification accuracy results. Only the CART classifier was significantly affected by the classification strategy used, since the direct classification turned out to be less accurate than the aggregation strategy for one of the feature vectors that was tested. It is worth noting that, for the case of direct classification, the target classes, pervious and impervious, were labelled in a binary way so more errors could be expected because only two classes could correspond to a large spectral variability. As opposed to CART, the SVM and NN classifiers were not sensitive to the large heterogeneity attributed to the target classes in the case of direct classification since they work in a more localized feature space (nearest neighbor or support vectors). On the other hand, the NN classifier used a large computational budget which, in contrast to SVM, was highly depended on the number of classes that were to be labelled, the number of training samples, as well as the support feature vector. In fact, NN was proved to be a non-efficient method when it is supported by "GLCM" texture features, especially if large areas have to be classified.

When the most suitable classification approach was selected, it was proved that the selection of an ad hoc training set was needed to accurately classify the remaining study area (aside from the pilot area) and to achieve a constant level of accuracy for all of the study area.

Finally, this work showed that the training sample selection should be carefully planned, because of the spectral variation, which is typical of archival aerial photographs. It has been proved that classification accuracy is notably affected by radiometric variation and also by an incorrect capture of the class variability for the entire area to be classified (poor spatial distribution of training samples). Therefore, an *ad hoc* training sample, which should be close to the area to be labelled, is recommended, including a good representation as well as enough samples for each subclass that constitute the pervious/impervious target classes.

Acknowledgment

The authors are grateful for the support of the GEOINCA research group of the University of Leon, Spain, which enabled the authors to develop this research work under its tutorship through a research visit. Thanks are especially due to D. Tammadge, also from the University of Leon (Spain), for his assistance with the preparation of the manuscript.

References

[1] Q. Weng, "Remote sensing of impervious surfaces in the urban areas: Requirements, methods, and trends," *Remote Sens. Environ.*, vol. 117, no. 15, pp. 34–39, Feb. 2012.

[2] N. Thomas, C. Hendrix, and R. G. Congalton, "A comparison of urban mapping methods using high-resolution digital imagery," *Photogramm. Eng. Remote Sens.*, vol. 69, no. 9, pp. 963–972, Sep. 2003.

[3] Q. Weng, "Modeling urban growth effects on surface runoff with the integration of remote sensing and GIS," *Environ. Manag.*, vol. 28, no. 6, pp. 737–748, Dec. 2001.

[4] R. R. Gillies, J. B. Box, J. Symanzik, and E. J. Rodemaker, "Effects of urbanization on the aquatic fauna of the Line Creek watershed, Atlanta – A satellite perspective," *Remote Sens. Environ.*, vol. 86, no. 3, pp. 411–422, Aug. 2003.

[5] E. T. Slonecker, D. B. Jennings, and D. Garofalo, "Remote sensing of impervious surfaces: A review," *Remote Sens. Rev.*, vol. 20, no. 3, pp. 227–225, Aug. 2001.

[6] T. R. Schueler, "The importance of imperviousness," *Watershed Protection Techniques*, vol. 1, no. 3, pp. 100–111, Mar. 1994.

[7] C. L. Arnold Jr. and C. J. Gibbons, "Impervious surface coverage: The emergence of a key environmental indicator," *J. Amer. Plan. Assoc.*, vol. 62, no. 2, pp. 243–258, Mar. 1996.

[8] E. Brabec, S. Schulte, and P. L. Richards, "Impervious surfaces and water quality: A review of current literature and its implications for watershed planning," *J. Plan. Liter.*, vol. 16, no. 4, pp. 499–514, May 2002.

[9] S. J. Goetz, R. K. Wright, A. J. Smith, E. Zinecker, and E. Schaub, "IKONOS imagery for resource management: Tree cover, impervious surfaces, and Riparian buffer analyses in the mid-Atlantic region," *Remote Sens. Environ.*, vol. 88, no. 1–2, pp. 195–208, Nov. 2003.

[10] Y. Zhou and Y. Q. Wang, "Extraction of impervious surface areas from high spatial resolution imagery by multiple agent segmentation and classification," *Photogramm. Eng. Remote Sens.*, vol. 74, no. 7, pp. 857–868, Jul. 2008.

[11] D. Lu and Q. Weng, "Extraction of urban impervious surfaces from an IKONOS image," *Int. J. Remote Sens.*, vol. 30, no. 5, pp. 1297–1311, Mar. 2009.

[12] J. E. Miller, S. A. C. Nelson, and G. R. Hess, "An object extraction approach for impervious surface classification with very-high-resolution imagery," *Prof. Geogr.*, vol. 61, no. 2, pp. 250–264, May 2009.

[13] M. E. Hodgson, J. R. Jensen, J. A. Tullis, K. D. Riordan, and C. M. Archer, "Synergistic use of lidar and color aerial photography for mapping urban parcel imperviousness," *Photogramm. Eng. Remote Sens.*, vol. 69, no. 9, pp. 973–980, Sep. 2003.

[14] L. Bruzzone and L. Carlin, "A multilevel context-based system for classification of very high spatial resolution images," *IEEE Trans. Geosci. Remote Sens.*, vol. 44, no. 9, pp. 2587–2600, Sep. 2006.

[15] A. S. Laliberte and A. Rango, "Texture and scale in object-based analysis of subdecimeter resolution unmanned aerial vehicle (UAV) imagery," *IEEE Trans. Geosci. Remote Sens.*, vol. 47, no. 3, pp. 1–10, Mar. 2009.

[16] S. W. Myint, P. Gober, A. Brazel, S. Grossman-Clarke, and Q. Weng, "Per-pixel vs. object-based classification of urban land cover extraction using high spatial resolution imagery," *Remote Sens. Environ.*, vol. 115, no. 5, pp. 1145–1161, May 2011.

[17] P. Treitz and P. J. Howarth, "High spatial resolution remote sensing data for forest ecosystem classification: An examination of spatial scale," *Remote Sens. Environ.*, vol. 72, no. 3, pp. 268–289, Jun. 2000.

[18] R. Pu, S. Landry, and Q. Yu, "Object-based urban detailed land cover classification with high spatial resolution IKONOS imagery," *Int. J. Remote Sens.*, vol. 32, no. 12, pp. 3285–3308, Jun. 2011.

[19] A. P. Carleer and E. Wolff, "Urban land cover multi-level region-based classification of VHR data by selecting relevant features," *Int. J. Remote Sens.*, vol. 27, no. 6, pp. 1035–1051, Mar. 2006.

[20] J. Im, J. R. Jensen, and J. A. Tullis, "Object-based change detection using correlation image analysis and image segmentation," *Int. J. Remote Sens.*, vol. 29, no. 2, pp. 399–423, Jan. 2008.

[21] D. Lu, S. Hetrick, and E. Moran, "Land Cover classification in a complex urban-rural landscape with QuickBird imagery," *Photogramm. Eng. Remote Sens.*, vol. 76, no. 10, pp. 1159–1168, Oct. 2010.

[22] T. Blaschke, "Object based image analysis for remote sensing," *ISPRS J. Photogramm. Remote Sens.*, vol. 65, no. 1, pp. 2–16, Jan. 2010.

[23] U. C. Benz, P. Hofmann, G. Willhauck, I. Lingenfelder, and M. Heynen, "Multi-resolution, object-oriented fuzzy analysis of remote sensing data for GIS-ready information," *ISPRS J. Photogramm. Remote Sens.*, vol. 58, no. 3–4, pp. 239–258, Jan. 2004.

[24] T. Blaschke and J. Strobl, "What's wrong with pixels? Some recent developments interfacing remote sensing and GIS," *GIS – Zeitschrift für Geoinformationssysteme*, vol. 14, no. 6, pp. 12–17, Jun. 2001.

[25] Y. Gao, J. F. Mas, B. H. P. Maathuis, Z. Xiangmin, and P. M. Van Dijk, "Comparison of pixel-based and object-oriented image classification approaches. A case study in a coal fire area, Wuda, Inner Mongolia, China," *Int. J. Remote Sens.*, vol. 27, no. 18, pp. 4039–4055, Sep. 2006.

[26] A. Dehvari and R. J. Heck, "Comparison of object-based and pixel based infrared airborne image classification methods using DEM thematic layer," *J. Geogr. Reg. Plan.*, vol. 2, no. 4, pp. 86–96, Apr. 2009.

[27] C. Cleve, M. Kelly, F. R. Kearns, and M. Moritz, "Classification of the wildland-urban interface: A comparison of pixel- and object-based classifications using high-resolution aerial photography," *Comput., Environ. Urban Syst.*, vol. 32, no. 32, pp. 317–326, Jul. 2008.

[28] T. G. Whiteside, G. S. Boggs, and S. W. Maier, "Comparing object-based and pixel-based classifications for mapping savannas," *Int. J. Appl. Earth Obs. Geoinf.*, vol. 13, no. 6, pp. 884–893, Dec. 2011.

[29] D. Lu and Q. Weng, "A survey of image classification methods and techniques for improving classification performance," *Int. J. Remote Sens.*, vol. 28, no. 5, pp. 823–870, Jan. 2007.

[30] G. Mountrakis, J. Im, and C. Ogole, "Support vector machines in remote sensing: A review," *ISPRS J. Photogramm. Remote Sens.*, vol. 66, no. 3, pp. 247–259, May 2011.

[31] M. Pal and P. M. Mather, "An assessment of the effectiveness of decision tree methods for land cover classification," *Remote Sens. Environ.*, vol. 86, no. 4, pp. 554–565, Aug. 2003.

[32] L. Samaniego, A. Bárdossy, and K. Schulz, "Supervised classification of remotely sensed imagery using a modified k-NN technique," *IEEE Trans. Geosci. Remote Sens.*, vol. 46, no. 7, pp. 2112–2125, Jul. 2008.

[33] L. Chandelier and G. Martinoty, "A radiometric aerial triangulation for the equalization of digital aerial images and orthoimages," *Photogramm. Eng. Remote Sens.*, vol. 75, no. 2, pp. 193–200, Feb. 2009.

[34] C. Song, C. E. Woodcock, K. C. Seto, M. P. Lenney, and S. A. Macomber, "Classification and change detection using Landsat TM data: When and how to correct atmospheric effects?," *Remote Sens. Environ.*, vol. 75, no. 2, pp. 230–244, Feb. 2001.

[35] F. Pacifici, F. Del Frate, C. Solimini, and W. J. Emery, "An innovative neural-net method to detect temporal changes in high-resolution optical satellite imagery," *IEEE Trans. Geosci. Remote Sens.*, vol. 45, no. 9, pp. 2940–2952, Sep. 2007.

[36] M. Chini, F. Pacifici, W. J. Emery, N. Pierdicca, and F. Del Frate, "Comparing statistical and neural network methods applied to very high resolution satellite images showing changes in man-made structures and rocky flats," *IEEE Trans. Geosci. Remote Sens.*, vol. 46, no. 6, pp. 1812–1821, Jun. 2008.

[37] C. Huang, C. Homer, and L. Yang, *Methods and Applications for Remote Sensing of Forests: Concepts and Case Studies*. Amsterdam, The Netherlands: Kluwer Academic, 2003, ch. 14, pp. 389–410.

[38] A. R. Gillespie, A. B. Kahle, and R. E. Walker, "Color enhancement of highly correlated images. II. Channel ratio and "chromaticity" transformation techniques," *Remote Sens. Environ.*, vol. 22, no. 3, pp. 343–365, Aug. 1987.

[39] T. Motohka, K. N. Nasahara, H. Oguma, and S. Tsuchida, "Applicability of green-red vegetation index for remote sensing of vegetation phenology," *Remote Sens.*, vol. 2, no. 10, pp. 2369–2387, Oct. 2010.

[40] J. A. Gamon and J. S. Surfus, "Assessing leaf pigment content and activity with a reflectometer," *New Phytologist*, vol. 143, no. 1, pp. 105–117, Jul. 1999.

[41] S. Gad and T. Kusky, "Lithological mapping in the eastern desert of Egypt, the Barramiya area, using Landsat thematic mapper (TM)," *J. African Earth Sciences*, vol. 44, no. 2, pp. 196–202, Feb. 2006.

[42] D. Chen, D. A. Stow, and P. Gong, "Examining the effect of spatial resolution and texture window size on classification accuracy: An urban environment case," *Int. J. Remote Sens.*, vol. 25, no. 11, pp. 2177–2192, Jun. 2004.

[43] F. Pacifici, M. Chini, and W. J. Emery, "A neural network approach using multi-scale textural metrics from very high-resolution panchromatic imagery for urban land-use classification," *Remote Sens. Environ.*, vol. 113, no. 6, pp. 1276–1292, Jun. 2009.

[44] F. Agüera, F. J. Aguilar, and M. A. Aguilar, "Using texture analysis to improve per-pixel classification of very high resolution images for mapping plastic greenhouses," *ISPRS J. Photogramm. Remote Sens.*, vol. 63, no. 6, pp. 635–646, Nov. 2008.

[45] M. Nagao and T. Matsuyama, "Edge preserving smoothing," *Comput. Graph. Image Process.*, vol. 9, no. 4, pp. 394–407, Apr. 1979.

[46] R. M. Haralick, K. Shanmugam, and I. Dinstein, "Textural features for image classification," *IEEE Trans. Syst., Man Cyber.*, vol. 3, no. 6, pp. 610–621, Nov. 1973.

[47] M. Herold, X. H. Liu, and K. C. Clarke, "Spatial metrics and image texture for mapping urban land use," *Photogramm. Eng. Remote Sens.*, vol. 69, no. 9, pp. 991–1001, Sep. 2003.

[48] D. A. Clausi, "An analysis of co-occurrence texture statistics as a function of grey level quantization," *Can. J. Remote Sens.*, vol. 28, no. 1, pp. 45–62, Feb. 2002.

[49] Q. Yu, P. Gong, N. Clinton, G. Biging, M. Kelly, and D. Schirokauer, "Object-based detailed vegetation classification with airborne high spatial resolution remote sensing imagery," *Photogramm. Eng. Remote Sens.*, vol. 72, no. 7, pp. 799–811, Jul. 2006.

[50] A. Baraldi and F. Parmiggiani, "Investigation of the textural characteristics associated with gray level co-occurrence matrix statistical parameters," *IEEE Trans. Geosci. Remote Sens.*, vol. 33, no. 2, pp. 293–304, Mar. 1995.

[51] G. Mallinis, N. Koutsias, M. Tsakiri-Strati, and M. Karteris, "Object-based classification using Quickbird imagery for delineating forest vegetation polygons in a Mediterranean test site," *ISPRS J. Photogramm. Remote Sens.*, vol. 63, no. 2, pp. 237–250, Mar. 2008.

[52] M. A. Friedl, C. E. Brodley, and A. H. Strahler, "Maximizing land cover classification accuracies produced by decision trees at continental to global scales," *IEEE Trans. Geosci. Remote Sens.*, vol. 37, no. 2, pt. 2, pp. 969–977, Mar. 1999.

[53] C. E. Brodley and M. A. Friedl, "Decision tree classification of land cover from remotely sensed data," *Remote Sens. Environ.*, vol. 61, no. 3, pp. 399–409, Sep. 1997.

[54] L. Breiman, J. H. Friedman, R. A. Olshen, and C. J. Stone, *Classification and Regression Trees*. Monterey, CA, USA: Wadsworth and Brooks, 1984.

[55] F. Esposito, D. Malerba, and G. Semeraro, "A comparative analysis of methods for pruning decision trees," *IEEE Trans. Pattern Anal. Mach. Intell.*, vol. 19, no. 5, pp. 476–491, Mar. 1997.

[56] T. Cover and P. Hart, "Nearest neighbor pattern classification," *IEEE Trans. Inf. Theory*, vol. 13, no. 1, pp. 21–27, Jan. 1967.

[57] J. M. Keller, M. R. Gray, and J. A. Givens, "Fuzzy k-nearest neighbor algorithm," *IEEE Trans. Syst., Man Cybern.*, vol. SMC-15, no. 4, pp. 580–585, Jul.-Aug. 1985.

[58] H. Zhu and O. Basir, "An adaptive fuzzy evidential nearest neighbor formulation for classifying remote sensing images," *IEEE Trans. Geosci. Remote Sens.*, vol. 43, no. 8, pp. 1874–1889, Aug. 2005.

[59] Q. Yu, P. Gong, N. Clinton, G. Biging, M. Kelly, and D. Schirokauer, "Object-based detailed vegetation classification with airborne high spatial resolution remote sensing imagery," *Photogramm. Eng. Remote Sens.*, vol. 72, no. 7, pp. 799–811, Jul. 2006.

[60] R. O. Duda and P. E. Hart, *Pattern Classification and Scene Analysis*. New York: Wiley, 1973.

[61] eCognition Document Version 1.2.1. Munich, Germany, Definiens Imaging, 2010.

[62] C. Huang, L. S. Davis, and J. R. G. Townshend, "An assessment of support vector machines for land cover classification," *Int. J. Remote Sens.*, vol. 23, no. 4, pp. 725–749, Feb. 2002.
[63] X. Huang and L. Zhang, "Road centreline extraction from high-resolution imagery based on multiscale structural features and support vector machines," *Int. J. Remote Sens.*, vol. 30, no. 8, pp. 1977–1987, Apr. 2009.
[64] G. Zhu and D. G. Blumberg, "Classification using ASTER data and SVM algorithms: The case study of Beer Sheva, Israel," *Remote Sens. Environ.*, vol. 80, no. 2, pp. 233–240, May 2002.
[65] F. Melgani and L. Bruzzone, "Classification of hyperspectral remote sensing images with support vector machines," *IEEE Trans. Geosci. Remote Sens.*, vol. 42, no. 8, pp. 1778–1790, Aug. 2004.
[66] J. Inglada, "Automatic recognition of man-made objects in high resolution optical remote sensing images by SVM classification of geometric image features," *ISPRS J. Photogramm. Remote Sens.*, vol. 62, no. 3, pp. 236–248, Aug. 2007.
[67] J. C. Trinder and M. Salah, "Support Vector Machines: Optimization and validation for land cover mapping using aerial images and lidar data," in *34th Int. Symp. Remote Sens.*, Sydney, Australia, 2011.
[68] V. N. Vapnik, *The Nature of Statistical Learning Theory*. New York: Springer-Verlag, 1995.
[69] C. Chang and C. Lin, "LIBSVM: A Library for support vector machines," *ACM Trans. Intell. Syst. Technol.*, vol. 2, May 2011.
[70] G. M. Foody, A. Mathur, C. Sanchez-Hernandez, and D. S. Boyd, "Training set size requirements for the classification of a specific class," *Remote Sens. Environ.*, vol. 104, no. 1, pp. 1–14, Sep. 2006.
[71] G. M. Foody and A. Mathur, "Toward intelligent training of supervised image classifications: Directing training data acquisition for SVM classification," *Remote Sens. Environ.*, vol. 93, no. 1–2, pp. 107–117, Oct. 2004.
[72] X. Zhuang, B. A. Engel, D. F. Lozano-Garcia, R. N. Fernandez, and C. J. Johannsen, "Optimization of training data required for neuro-classification," *Int. J. Remote Sens.*, vol. 15, no. 16, pp. 3271–3277, Aug. 1994.
[73] R. G. Congalton, "A review of assessing the accuracy of classifications of remotely sensed data," *Remote Sens. Environ.*, vol. 37, no. 1, pp. 35–46, Jul. 1991.
[74] J. R. Jensen, *Introductory Digital Image Processing: A Remote Sensing Perspective*, 2nd ed. New York: Prentice Hall, 1996.
[75] R. G. Congalton and K. Green, *Assessing the Accuracy of Remotely Sensed Data*, 2th ed. Boca Raton, FL, USA: CRC Press, 2009.
[76] J. Sauro and J. R. Lewis, "Estimating completion rates from small samples using binomial confidence intervals: Comparisons and recommendations," in *Proc. Human Factors and Ergonomics Soc.*, Orlando, FL, USA, 2005, pp. 2100–2104.
[77] D. Lu, S. Hetrick, and E. Moran, "Impervious surface mapping with QuickBird imagery," *Int. J. Remote Sens.*, vol. 32, no. 9, pp. 2519–2533, May 2011.
[78] H. G. Jones and R. A. Vaughan, *Remote Sensing of Vegetation: Principles, Techniques, and Applications*. Oxford, U.K.: Oxford Univ. Press, 2010.
[79] L. Soh and C. Tsatsoulis, "Texture analysis of SAR sea ice imagery using gray level co-occurrence matrices," *IEEE Trans. Geosci. Remote Sens.*, vol. 37, no. 2, pp. 780–795, Mar. 1999.
[80] P. Maillard, "Comparing texture analysis methods through classification," *Photogramm. Eng. Remote Sens.*, vol. 69, no. 4, pp. 357–367, Apr. 2003.
[81] L. Wang, W. P. Sousa, P. Gong, and G. S. Biging, "Comparison of IKONOS and QuickBird images for mapping mangrove species on the Caribbean coast of Panama," *Remote Sens. Environ.*, vol. 91, no. 3–4, pp. 432–440, Jun. 2004.

Ismael Fernández Luque received the B.S. degree in cartography and geodesy engineering from the Polytechnic School of Jaen, Spain, in 2009. Since 2009, he has been working towards the Ph.D. degree in geomatic engineering applied to the evaluation of natural resources at the University of Almería, Spain.

His current interests include coastal areas management, shoreline extraction and evolution assessment. His other field of work is the application of remote sensing on coastal areas, including LiDAR data analysis, photogrammetric processes, and high spatial resolution satellite imagery DEM extraction and orthorectification.

Fernando J. Aguilar received the Ph.D. degree from Cordoba University, Spain, in 1997.

He is currently a Senior Lecturer at Almeria University, Spain, working with the Department of Agricultural Engineering. At present, he is the Head of the Research Group called "Integrated Landscape Management and Spatial Information Technologies", leading an Excellence Research Project entitled "Multisource geospatial data integration and mining for the monitoring and modelling of coastal areas evolution and vulnerability: Applied to a pilot area located at Levante de Almería, Spain". His field interests are related to digital elevation models, remote sensing, digital photogrammetry and GIS. Author of several international publications, he is also a peer-reviewer of many of GIS and remote sensing journals.

Flor Alvarez received the Ph.D. degree from the University of Vigo, Spain, in 2006.

She currently works as an Assistant Professor at the University of León, Spain, in the Department of Mining Engineering. Her main research area is monitoring natural resources using remote sensing. She has led research projects which involve the calibration and use of digital aerial photographs to monitor biomass. Her other research fields are segmentation, calibration of aerial images, and GIS. She has been a guest researcher at the Pacific Forestry Centre (Canada) and at the ITC (The Netherlands). She is a co-author of several international publications and is a peer reviewer of several GIS and remote sensing journals.

Manuel Ángel Aguilar received Agricultural Engineering and Ph.D. degrees from the University of Córdoba, Spain, in 1996 and 2001, respectively.

Since 1999, he has been a Professor of technical drawing at the Almería Engineering High School of University of Almería (Spain). He is currently a Senior Lecturer in this University, working with the Department of Agricultural Engineering. His fields of interest are close-range, satellite and classic digital photogrammetry, remote sensing of land cover, as well as the generation and quality control of DEMs. His recent research has focused on the latest breed of Very High Resolution satellite imagery from GeoEye-1 and WorldView-2.